Astronomy & Astrophysics manuscript no. rbonito
December 14, 2009

© ESO 2009

arXiv:0912.2757v1 [astro-ph.SR] 14 Dec 2009

Generation of radiative knots in a randomly pulsed protostellar jet

I. Dynamics and energetics

R. Bonito[1,2], S. Orlando[2], G. Peres[1,2], J. Eislöffel[3], M. Miceli[1,2], and F. Favata[4]

[1] Dip. Scienze Fisiche ed Astronomiche, Sez. Astronomia, Università di Palermo, P.zza del Parlamento 1, 90134 Palermo, Italy
[2] INAF – Osservatorio Astronomico di Palermo, P.zza del Parlamento 1, 90134 Palermo, Italy
[3] Thüringer Landessternwarte, Sternwarte 5, D-07778 Tautenburg, Germany
[4] European Space Agency Community Coordination and Planning Office 8-10 rue Mario Nikis F-75738 Paris cedex 15 France

Received, accepted

Abstract

Context. Herbig-Haro objects are characterized by a complex knotty morphology detected mainly along the axis of protostellar jets in a wide range of bands: from radio to IR to optical bands, with X-rays knots also detected in the last few years. Evidence of interactions between knots formed in different epochs have been found, suggesting that jets may result from the ejection of plasma blobs from the stellar source.
Aims. We aim at investigating the physical mechanism leading to the irregular knotty structure observed in protostellar jets in different wavelength bands and the complex interactions occurring among blobs of plasma ejected from the stellar source.
Methods. We perform 2D axisymmetric hydrodynamic numerical simulations of a randomly ejected pulsed jet. The jet consists of a train of blobs which ram with supersonic speed into the ambient medium. The initial random velocity of each blob follows an exponential distribution. We explore the ejection rate parameter in order to derive constraints on the physical properties of protostellar jets by comparison of model results with observations. Our model takes into account the effects of radiative losses and thermal conduction.
Results. We find that the mutual interactions of blobs ejected at different epochs and with different speed lead to a variety of plasma components not described by current models of jets. The main features characterizing the random pulsed jet scenario are: single high speed knots, showing a measurable proper motion in nice agreement with optical and X-rays observations; irregular chains of knots aligned along the jet axis and possibly interacting with each other; reverse shocks interacting with outgoing knots; oblique shock patterns produced by the reflection of shocks at the cocoon surrounding the jet. All these structures concur to determine the morphology of the jet in different wavelength bands. We also find that the thermal conduction plays a crucial role in damping out hydrodynamic instabilities that would develop within the cocoon and that contribute to the jet breaking.

Key words. Hydrodynamics; ISM: Herbig-Haro objects; ISM: jets and outflows; X-rays: ISM

1. Introduction

Herbig-Haro (HH) objects characterize the emission regions near protostars where the accretion process is still ongoing, often allowing us to identify the presence of a young stellar object (YSO) not observable otherwise. The HH objects are observed in all wavelength bands (from radio and IR to optical and UV, and also in the X-rays; see the review of Reipurth & Bally 2001) as a chain of knots within the supersonic protostellar jets. The knotty structure has been frequently observed in the optical band in many HH objects and has been discovered for the first time also in X-rays in HH 154 (Favata et al. 2006, Bonito et al. 2008), one among the nearest and most luminous X-ray emitting protostellar jets. The HH 154 jet is one of the best studied, being observed through multi-wavelength and multi-epoch observations with several instruments, among them the Hubble Space Telescope (HST; Fridlund & Liseau 1998; Bonito et al. 2008), Chandra/ACIS-I (Bally et al. 2003; Favata et al. 2006), and XMM-Newton (Favata et al. 2002).

The origin of chains of optical knots commonly observed in jets have been traditionally interpreted through models of jet ejected with a sinusoidal variable velocity (e.g. Raga et al. 2007). In fact, in these models, the internal shocks resulting from plasma flowing with different velocity lead to a nodular structure, constituted by a regular chain of knots with individual proper motions. An alternative scenario has been proposed

---

Send offprint requests to: R. Bonito
e-mail: `sbonito@astropa.unipa.it`

by Yirak et al. (2009) who model, through 3D simulations, the appearing of clumps within the jet beam (with random locations, sizes, and speeds), and explore the possibility of intrinsic density heterogeneity of the jet. Original models of jets accounting for stochastic jets and random time variability have been previously discussed by Roberts (1986) (in the context of extragalactic jets) and Raga (1992) (in the limit of large distances from the stellar source). Also Vitorino et al. (2002) suggested a disk/jet launching model with a combination of a continuous and a random component of the velocity, thus justifying the random speed models.

Recently, multi-wavelength observations of HH 154 collected in 2005 with both Chandra and HST showed evidence of mutual interactions between bright knots, formed probably at different epochs and with different speeds (Bonito et al. 2008). These features seem to be common also in other objects (Garatti et al. 2009) and are not predicted in models of jets with sinusoidal velocity. Moreover as discussed by Yirak et al. (2009), the observed knots could be interpreted erroneously as the product of a sinusoidal variable velocity jet.

The aim of this work is to investigate, through detailed numerical modeling, the origin and dynamics of the irregular knotty structure observed in several bands (and, in particular, in X-rays) in protostellar jets and the possible interactions between knots. Moreover, we aim at deriving general model predictions to be compared with observations of X-ray emitting protostellar jets (DG Tau, HH 2, etc.) to understand the physical mechanisms leading to X-ray emission in different objects.

In our previous studies, we have investigated the origin of X-ray emission from protostellar jets, through a model of a continuously ejected supersonic jet (Bonito et al. 2004, Bonito et al. 2007). Such a model predicts the propagation of a compact X-ray source through the circumstellar medium with spectral behavior, X-ray luminosity, and proper motion in good agreement with the observations (Favata et al. 2002). However, the model does not reproduce the complex knotty morphology and variability of the X-ray source detected in HH 154 (Favata et al. 2006).

Here we suggest an improvement to our previous model by considering the scenario of a pulsed jet interacting with an initially homogeneous ambient medium. The model presented here describes a jet constituted by a train of plasma blobs randomly ejected by the stellar source. The initial velocity of our model follows an exponential distribution and this choice corresponds to a distribution of many low-speed blobs and few blobs with high initial ejection velocity. The blobs are expected to interact with each other leading to the formation of knots with individual proper motions, possibly observable in various bands. In the following, we will refer to blobs to consider the plasma ejected from the stellar source and to knots to consider the observable structures within the jet.

We plan to present our results in two papers. In the present paper we describe the dynamics and energetic of the pulsed jet/ambient interaction, exploring the influence of the ejection rate of plasma blobs. In the second paper (Bonito et al. 2009, in preparation) we will focus on the variability and morphology of X-ray emitting features predicted by the model as they would be observed with Chandra/ACIS-I and with XMM/Newton.

The paper is organized as follows: in Sect. 2 we describe the numerical model of the pulsed jet, its initial setup, and the exploration of the parameter space; in Sect. 3 we analyze the hydrodynamic evolution of the model, focusing on the internal structures occurring within the jet, and the physical effects due to the thermal conduction process; in Sect. 4 we discuss the results and their physical interpretation, and in Sect. 5 we draw our conclusions.

2. The model

The model describes a protostellar jet ramming with a supersonic variable ejection speed into an initially homogeneous ambient medium. The fluid is assumed to be fully ionized[1] with a ratio of specific heats $\gamma = 5/3$. The model takes into account the radiative cooling from optically thin plasma, and the thermal conduction (including the effects of heat flux saturation). The propagation of the jet through the surrounding medium is modeled by solving numerically the time-dependent hydrodynamic equations:

$$\frac{\partial \rho}{\partial t} + \nabla \cdot \rho \mathbf{v} = 0 \tag{1}$$

$$\frac{\partial \rho \mathbf{v}}{\partial t} + \nabla \cdot \rho \mathbf{v}\mathbf{v} + \nabla p = 0 \tag{2}$$

$$\frac{\partial \rho E}{\partial t} + \nabla \cdot (\rho E + p)\mathbf{v} = -\nabla \cdot q - n_e n_H P(T) \tag{3}$$

with

$$p = (\gamma - 1)\rho\epsilon\,, \qquad E = \epsilon + \frac{1}{2}|\mathbf{v}|^2\,,$$

where p is the pressure, E the total gas specific energy (internal energy, ϵ, and kinetic energy) respectively, ρ is the mass density, t the time, $\mathbf{v}$ the plasma velocity, q the heat flux, n_e and n_H are the electron and hydrogen density, respectively, $P(T)$ is the radiative losses function per unit emission measure[2], T the plasma temperature.

Following Dalton & Balbus (1993), we use an interpolation expression for the thermal conductive flux which allows for a smooth transition between the Spitzer (Spitzer 1962) and saturated (Cowie & McKee 1977) conduction regimes

$$q = \left(\frac{1}{q_{\rm spi}} + \frac{1}{q_{\rm sat}}\right)^{-1}\,, \tag{4}$$

where

$$q_{\rm spi} = -\kappa(T)\nabla T\,, \tag{5}$$

where $\kappa(T) = 9.2 \times 10^{-7} T^{5/2}$ erg s^{-1} K^{-1} cm^{-1} is the thermal conductivity, and

$$q_{\rm sat} = -sign(\nabla T) 5\phi\rho c_{\rm s}^3\,, \tag{6}$$

---

[1] See Bonito et al. 2007.

[2] $P(T)$ is described by a functional form that takes into account free-free, bound-free, bound-bound and 2 photons emission (see Raymond & Smith 1977; Mewe et al. 1985; Kaastra & Mewe 2000).

where $\phi \sim 0.3$ (Giuliani 1984; Borkowski et al. 1989, and references therein) and $c_{\rm s}$ is the isothermal sound speed.

The hydrodynamic equations are solved using the FLASH code (Fryxell et al. 2000) with customized numerical modules for the optically thin radiative losses and the thermal conduction (see Orlando et al. 2005, for the details of the implementation of the thermal conduction). The FLASH code uses a directionally split Piecewise Parabolic Method (PPM) solver to handle compressible flows with shocks (Colella & Woodward 1984), the PARAMESH library to handle adaptive mesh refinement (MacNeice et al. 2000), and the Message-Passing Interface library to achieve parallelization.

2.1. Numerical setup

We solve the hydrodynamic equations in 2D, using cylindrical coordinates in the plane (r, z), and assuming axisymmetry with the jet axis coincident with the axis of symmetry (z). The computational grid size is (2000 AU × 6000 AU). The maximum spatial resolution achieved by our simulations is ≈ 8 AU, as determined with the algorithm of the PARAMESH library for 4 refinement levels, which corresponds to covering the initial jet radius with 4 points at the maximum resolution [3].

We follow the evolution of the jet for a time interval ranging between 100 and 400 yrs, depending on the set of model parameters. The pulsed jet consists of a train of blobs, each lasting for 0.5 yr, with an ejection rate corresponding to a time interval between two consecutive blobs Δt. Each blob is ejected with a random velocity directed along the jet axis following an exponential distribution

$$v(r=0,t) = v_{jMAX}(b - log(rand(t) - a)) \ , \tag{7}$$

where

$$b = log\frac{1}{1-e^{-1}} \ , \tag{8}$$

$$a = \frac{e^{-1}}{e^{-1}-1} \ , \tag{9}$$

and $rand$ is a number ranging between 0 and 1 obtained using a random number generator. The maximum velocity of the blobs is $v_{jMAX} = 4680$ km/sec and corresponds to the highly supersonic initial Mach number $M = 1000$. Fig. 1 shows the initial velocity values of each blob ejected with an ejection rate corresponding to Δt = 2 yr. We generated the random seed once for all the runs so the values follow always the same sequence, only the rate is different.

The initial random velocity of each blob is along the z axis, coincident with the jet axis, and its radial profile is

$$v(r,t) = \frac{v(r=0,t)}{\nu \cosh(r/r_j)^w - (\nu - 1)} \ , \tag{10}$$

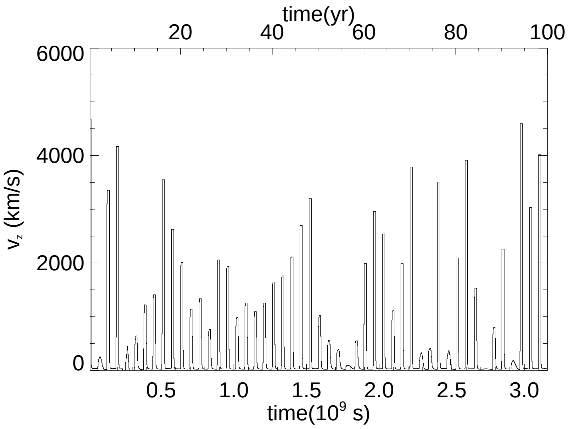

Figure 1. Initial jet velocity of each blob as a function of time for the Δt = 2 yr case (run LJ2).

where $v(r=0,t)$ is the on-axis velocity, ν is the ambient-to-jet density ratio, $r_{\rm j}$ is the initial jet radius and $w = 4$ is the steepness parameter for the shear layer which allows a smooth transition of the kinetic energy at the interface between the jet and the ambient medium. This layer avoids the growth of random perturbation at the jet border (Bodo et al. 1994). The density profile as a function of the radial direction is

$$\rho(r) = \rho_j \left(\nu - \frac{\nu - 1}{\cosh(r/r_j)^w} \right) \ , \tag{11}$$

where $\rho_{\rm j}$ is the jet density (see also the velocity and density profiles as a function of the radial distance from the axis in Bonito et al. 2007, Fig. 1).

Reflection boundary conditions are imposed along the jet axis (consistent with the adopted symmetry), inflow boundary conditions at the base for $r < r_j$, where r is the radial distance in cylindrical coordinates and r_j is the jet radius, and outflow boundary conditions elsewhere.

2.2. Parameter space

The model parameters are derived from the optical and X-ray data analysis of protostellar jets (e.g. Podio et al. 2006; Bonito et al. 2008; Favata et al. 2006) and from the results of previous models (Bonito et al. 2004, 2007). Tab. 1 summarizes the physical parameters characterizing the simulations.

The exploration of the parameter space mainly focuses on the ejection rate of the blobs composing the jet. In all our simulations, we impose the initial radius and density of the blobs, namely $r_j \approx 30$ AU and $n_j = 500$ cm^{-3}, respectively. For the sake of completeness, we explore both the initial light jet scenario (a jet initially less dense than the unperturbed ambient medium), and the initial heavy jet scenario (a jet initially denser than the ambient medium); we consider, therefore, initial ambient-to-jet density ratio $\nu = n_a/n_j = 0.1, 10$ in the heavy and light jet cases, respectively. The initial blob temperature T_j ranges between 10^2 and 10^4 K, while the ambient temperature, T_a, is derived assuming initial pressure equilibrium between the jet and the unperturbed ambient.

---

[3] The maximum resolution corresponds to ≈ 8 times the resolution of Chandra/ACIS-I observations and to about twice the spatial resolution of HST, 0.4”≈ 60 AU at 150 pc and 0.1”≈ 15 AU at 150 pc, i.e. at the distance of the nearest star forming region in Taurus.

Table 1. Summary of the initial physical parameters characterizing the simulations: Δt is the time between two consecutive blobs, ν is the ambient-to-jet density contrast, M is the initial jet Mach number, $v_{\rm j}$ is the velocity of each ejected blob (here we indicate the range of values randomly generated in our model), $T_{\rm j}$ is the initial jet temperature, $n_{\rm a}$ is the ambient density. In all the models we assume: $r_{\rm j} = 30$ AU as initial jet radius, $n_{\rm j} = 500$ cm^{-3} as initial jet density, and $T_{\rm a} = 10^3$ K as initial ambient temperature.

Model	Δt yr	ν	M	$v_{\rm j}$ [km s^{-1}]	$T_{\rm j}$ [10^4 K]	$n_{\rm a}$ [cm^{-3}]
LJ0.5	0.5	10	1000	$10 - 4700$	10^4	5000
LJ2	2	10	1000	$10 - 4700$	10^4	5000
LJ8	8	10	1000	$10 - 4700$	10^4	5000
LJ2RD	2	10	1000	$10 - 4700$	10^4	5000
HJ2	2	0.1	300	$10 - 1400$	10^2	50

The initial jet Mach number values are $M = v_{\rm j}/c_{\rm a} = 300$ in the heavy jet case and 1000 in the light jet case, and corresponds to a maximum velocity of the first blob of about 5000 km/s. Note that we are interested on the evolution of the pulsed jet after a transient phase, i.e. after the first ejected blob of plasma has perturbed the ambient (which is no more homogeneous). We require, therefore, a high speed of the first blob in order to perturb quickly the computational domain (6000 AU). The speed of each ejected blob ranges between about 10 km/s and 5000 km/s during the evolution of the pulsed jet. It is worth noting that the apparently high values of the maximum ejection velocity cannot be compared directly to the observable speeds of the knots within the protostellar jets. In fact we have chosen the initial speeds which lead, once the interaction between the ejected plasma and the ambient medium has taken place, to the observed knots speed of a few hundred km/s (Fridlund & Liseau 1998; Bonito et al. 2008).

Since the optical knots in HH jets, in general, show timescale variability of a few years (see morphological evolution of the HH 154 jet in about 2 yr discussed in Bonito et al. 2008), with new knots appearing at the base of the jet in about 2 yr (e.g. HH 1 and HH 34, see the movies discussed in Hartigan 2003), we have chosen an initial ejection rate parameter corresponding to a time interval Δt = 2 yr between two consecutive blobs. Then we explore this parameter taking into account a 1/4 value (Δt = 0.5 yr) and a $\times 4$ value (Δt = 8 yr) in order to constrain the ejection rate from the comparison between our model predictions and the observations.

3. Results

3.1. Hydrodynamic evolution

In all our simulations, the jet propagates through the homogeneous ambient medium, forming a cocoon, and shows a complex density structure inside. The ejection rate determines the energy powering the jet and, in fact, the maximum distance from the driving source reached at a given epoch in runs LJ0.5, LJ2, and LJ8 strongly varies. As shown in Fig. 2, the low ejection rate case (LJ8) travels through 3000 AU in 100 yr, while the high ejection rate cases reach the 6000 AU distance in less than 90 yr (LJ2) or even less than 50 yr (LJ0.5), being the kinetic power released in these cases much higher than in LJ8.

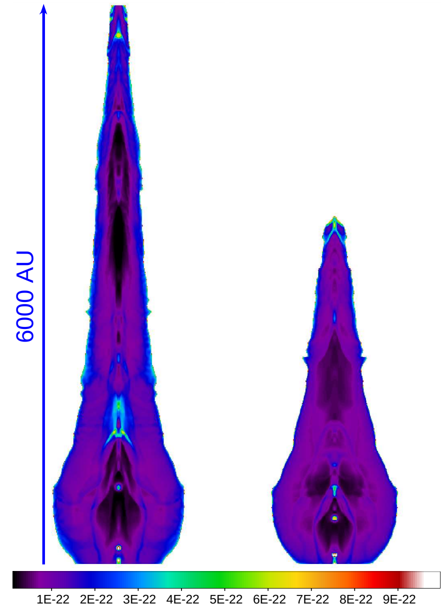

Figure 2. 2D spatial distributions of the density of the jet/ambient interaction in runs LJ2 (left semi-panel) and LJ8 (right semi-panel). The head of the jet leaves the domain after about 90 yr in LJ2 whereas in LJ8 it does not reach the end of the domain (6000 AU) in 100 yr.

Although the ambient medium is initially homogeneous, it becomes quickly inhomogeneous as the first and consecutive blobs ejected by the stellar source interact with it. Fig. 3 shows a cut along the jet axis of the density (upper panel) and of the temperature (lower panel) distributions. The whole computational domain (6000 AU) is filled with several structures, with the density varying by more than two orders of magnitude. Also the thermal conditions vary along the jet axis, so that the sound speed and the Mach number are not uniform. As a result, strong variations of the shock velocities ($v_{sh} \propto \rho^{-1/2}$) and of the post-shock properties are determined due to the varying pre-shock conditions. Note that, at variance with the model of a continuous jet, in our pulsed jet model the density contrast between the ambient medium and the blob can vary during the jet/ambient evolution. As discussed above, in a few years, the medium is so complex that, even if the initial density of the ejected blobs does not vary ($n_{\rm j} = 500$ cm^{-3}, see the red dashed line superimposed in the upper panel of Fig. 3), the ambient density strongly varies during the evolution thus leading to several different scenarios in which the ejected blob could be denser or less dense than the surrounding medium (see upper panel in Fig. 3).

It is worth emphasizing that the random velocity of the blobs ejected at different epochs together with the strongly inhomogeneous medium in which each blob (except the first one) propagates, lead to complex mutual interactions of the blobs. The frequency of mutual interactions within the jet depends on the ejection rate, being the largest in run LJ0.5 and the lowest

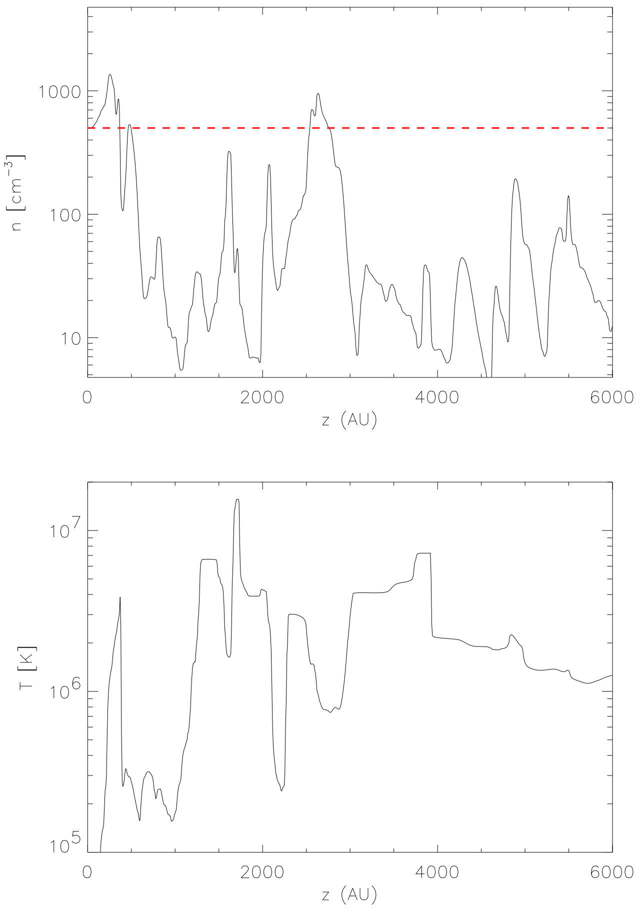

Figure 3. Cut along the jet axis of the spatial distributions of density (upper panel) and of temperature (lower panel) in run LJ0.5: the chain of knots within the jet due to previously ejected blobs lead to a complex structure of the medium where the new blobs are ejected. The red dashed line superimposed in the density profile indicates the initial jet density value ($n_{\rm j} = 500$ cm^{-3}).

in run LJ8. These interactions result in a rich variety of plasma structures that cannot be described by current models of jet and that determine an irregular pattern of knots. In the following, we illustrate the common features that may contribute in determining the morphology of the pulsed jet by analyzing the density and temperature spatial distributions and evolution.

The most evident feature predicted by our model is an irregular chain of knots aligned along the jet axis. Depending on the model parameters, the knots may emit mainly either in the optical band or in the X-ray band. In the former case, the chain of (optical) knots can be highlighted by deriving density maps of plasma with temperature ranging between $(5000-100000)$ K, which is a proxy of optical emission. To this end, we first reconstruct the 3D spatial distributions of mass density and temperature, according to the symmetry of the problem; then, assuming the jet traveling perpendicularly to the line-of-sight (LoS), we integrate the density along the LoS and derive the 2D density maps. As an example, Fig. 4 shows an enlargement of the base of the jet for run HJ2, i.e. in the heavy jet scenario (see Tab. 1), where a chain of (optical emitting) knots within the jet is well visible. These knots show a detectable proper motion in a few years, in good agreement with typical observations of the moving optical knots within protostellar jets. In particular, by measuring the spatial displacement of the center of the circular region identifying the E knot in Fig. 4 in the time interval $(45-50)$ yr, we derive an average knot speed along the jet axis of about 600 km/s, in nice agreement with the values obtained from the optical observations of the knots within protostellar jets (Fridlund et al. 2005; Bonito et al. 2008, Eislöffel et al. 1994). In this case, we find evidence of knotty structures analogous to those observed in protostellar jets, with a chain of several subsequent knots in a few hundreds AU from the stellar source.

Similar patterns of knots but emitting mainly in the X-ray band (see Bonito et al., 2009, in preparation) are found in the light jet scenario when the ejection rate is high ($\Delta t = 0.5, 2$ yr), as shown in the 2D spatial distribution of mass density in Fig. 5. In particular several dense structures are well visible within the jet, mainly on the jet axis.

The spatial separation between two consecutive knots is neither uniform in space nor constant in time in all the different cases analyzed because of the variation of the blob speed and of the medium surrounding the blob. This leads to a complex pattern consistent with observations of several protostellar jets, among them HH 154 (see Bonito et al. 2008). Sinusoidal ejection velocity models usually show a chain of knots with an almost regular pattern (Raga et al. 2007) within the jet which does not reproduce the observed structure of complex jets, (e.g. HH 1, Reipurth et al. 2000; HH 111 Hartigan et al. 2001).

The knots resulting from the interactions among ejected blobs have, in general, different proper motions and may ultimately interact with each other. In some cases, high speed knots can interact with the head of the jet, possibly overtaking the cocoon, and thus traveling into the unperturbed ambient medium. A random variability of the injection velocity of the blobs and the consequent catching-up processes between knots have been discussed previously by Raga (1992). This effect is evident in Fig. 4, where the initially separated C and B knots merge in a single structure (named $C+B$ in the figure). Analogously the density cut along the jet axis indicate that the two peaks C and B at $t \approx 45$ yr of evolutionary stage (upper panel of Fig. 6), correspond to a single peak $C+B$ after 5 yr (lower panel of Fig. 6). These features have been observed in several HH jets (Bonito et al. 2008; Garatti et al. 2009).

Analogous clump-clump interactions and high speed knots overtaking the head of the jet (including also the case of off-axis structures) have been found by Yirak et al. (2009), although these authors have not considered any proxy of optical emission as done here. Note, however, that the knots in Yirak et al. (2009) are the result of imposed inhomogeneities of the jet flow (describing the effect of possible instabilities) and their characteristic size is lower than the jet diameter (subradius), whereas in our model the knots are the result of the pulsed ejection of the jet (possibly related to accretion phenomena) and their size is comparable to the jet diameter. Note, also, that Yirak et al. (2009) considered ranges of temperatures and velocities smaller than those discussed here and their model

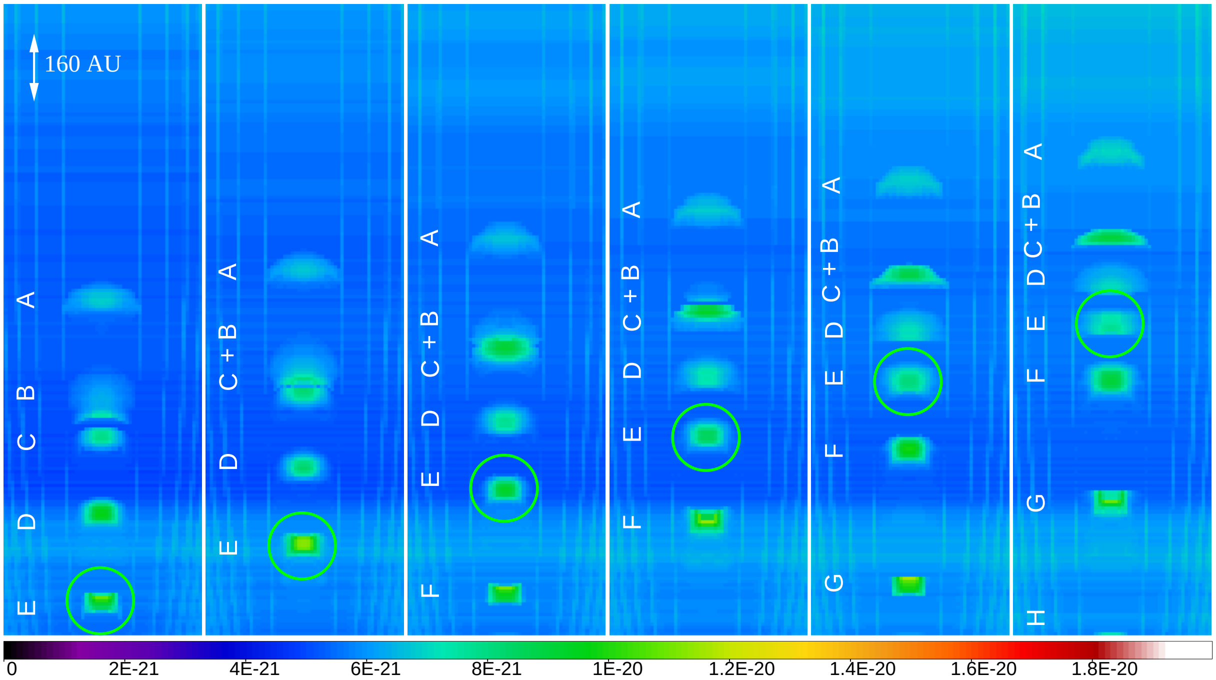

Figure 4. Density maps of plasma with temperature ranging between $(5000 - 100000)$ K (a proxy of optical emission) for the model HJ2. The green circles (of radius ≈ 80 AU) superimposed to each frame mark the position of a specific knot as it evolves in time: the proper motion is detectable in a few years, the time-lapse between two consecutive frames is 1 yr.

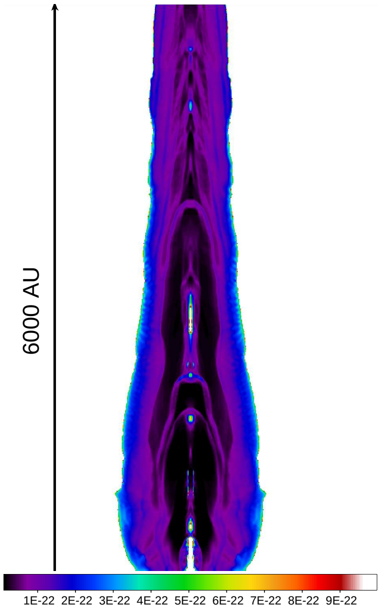

Figure 5. 2D spatial distribution of the density of the jet/ambient interaction in model LJ0.5: a chain of several knots arises due to blobs ejected at different epochs.

does not take into account the thermal conduction effects. As discussed below in Sect. 3.2, our simulations show that the thermal conduction plays a crucial role in damping out the hydrodynamic instabilities that would develop within the jet, leading to a faster and more collimated jet.

Another important feature produced by our model is associated with the formation of reverse shocks moving in the opposite direction with respect to the ejected blobs and interacting with these (see Fig. 7). This interaction produces, under certain circumstances, the formation of shocks with no detectable proper motion over time scales of a few years, as observed, for instance, in the X-ray source of HH 154 (Favata et al. 2006). The collision between knots and reverse shocks is a feature common to all the ejection rates discussed here and occurs several times during the time covered in our simulations. As an example, Fig. 7 shows one of these occurrence for run LJ0.5. In the first panel, the reverse shock is located ≈ 1200 AU above the source driving the jet and the knot traveling towards it is initially at about 200 AU from the source. As the jet evolves, the knot reaches a distance of ≈ 800 AU from the source, with the reverse shock just ≈ 200 AU above it. After about two years the two structures interact at a distance of ≈ 1000 AU from the source and the shock location does not change appreciably over a timescale of few years.

A more complex morphology arises when the reverse shock is reflected obliquely by the cocoon, leading, in this case, to an oblique shock pattern. Fig. 8 shows the evolution of an oblique shock in a few years, moving from the external cocoon toward the jet axis, as indicated by the arrows superimposed on each frame. Note that the propagation of the oblique shock causes the formation of a dense and well collimated core within the jet itself as evident in the last frame of Fig. 8.

3.2. *Effects of the thermal conduction*

Our model takes into account both the radiative losses from an optically thin plasma and the thermal conduction, in Spitzer or in saturated regimes. It is interesting, therefore, to investigate

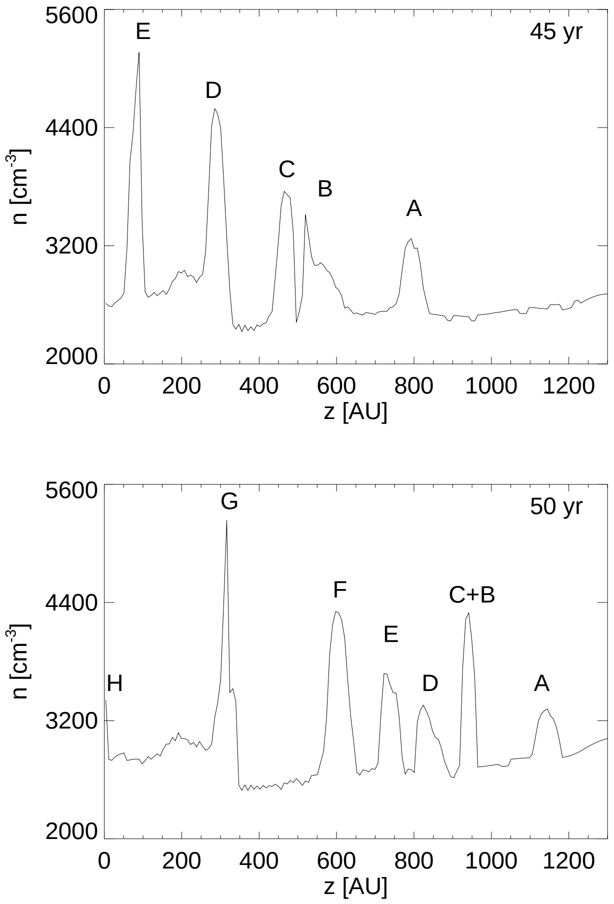

Figure 6. Cuts along the jet axis of the first (upper panel) and the last (lower panel) frame of Fig. 4, corresponding to 45 yr and 50 yr since the beginning of the jet/ambient interaction. In a few years, the proper motion of the knots within the jet, the interaction between knots, and the generation of new knots are well visible.

the effects of the thermal conduction in the dynamics and energetic of the jet. These effects are highlighted by comparing simulations either with or without the thermal conduction. To this end, we performed an additional run with setup identical to that used for run LJ2 but without the thermal conduction (run LJ2RD). We find that, in run LJ2RD, the maximum distance from the stellar source is significantly smaller than that in run LJ2. As an example, Fig. 9 shows the temperature distributions in the two cases after the first blob has reached the upper boundary of the computational domain, namely at $t \approx 90$ yr in LJ2 and at $t \approx 350$ yr in LJ2RD. We found, therefore, that the jet travels more slowly into the ambient medium if the thermal conduction effects are inhibited. In fact, in LJ2RD, the jet evolution is dominated by thermal and hydrodynamic instabilities (see right panel in Fig. 9) that are known to contribute to the jet breaking. Conversely, these instabilities are damped out by the thermal conduction in run LJ2, and the jet propagates to larger distances.

The comparison between the two temperature maps of runs LJ2 and LJ2RD in Fig. 9 indicate also significant differences in the morphology due to the presence of the thermal conduction. In fact, beside the different evolutionary stages needed in the two cases in order to reach the top of the computational domain, it is also evident how the thermal conduction leads to a smooth and more collimated spatial distribution of temperature. The radiative case LJ2RD shows a significant radial spread of the temperature distribution, accounting for the decelerated material traveling into the instabilities.

4. Discussion

4.1. Observable proper motion

As discussed in Bonito et al. (2007), the high initial jet velocity is not an observable since we can measure just the speed of formed knots, i.e. the velocity of the plasma structures formed by the interactions among the blobs or of the blobs with the inhomogeneous surrounding medium. In other words, we can observe the effect of jet/ambient interaction, not the launching region itself. We are interested, therefore, in deriving the average speed of the observable knots, determining the internal density structure of the jet. To this end, Fig. 10 shows the density-weighted average of the $z-$component of the plasma bulk velocity within a distance of 10 pixels[4] from the jet axis for the three ejection rates analyzed (runs LJ0.5, L2, L8). The velocity values are consistent with typical knots speeds observed within optical jets (few hundreds km/s, Eislöffel & Mundt 1998; Bally et al. 2003; Bonito et al. 2008). In particular we find a very good agreement for the $\Delta t = 2$ yr case and the speed value decreases with increasing Δt parameter.

Following our model results, we can make predictions about the initial ejection velocity leading to the observed speed. In order to verify if our assumed values are reasonable, we can compare the mechanical luminosity derived from our simulations with the observed bolometric luminosity of the source of the HH 154 jet. In particular, from the values of the initial velocity used here and shown in Tab. 1 and following the relation (18) in Bonito et al. (2007), the kinetic power derived from our model ranges between $L_{\rm mech} \sim 10^{-7} - 10\ L_{\odot}$, i.e. always below the observed bolometric luminosity of the source of the HH 154 jet, $L_{bol} \approx 40\ L_{\odot}$ (see Bonito et al. 2007, Tab. 1). Thus we conclude that the initial blob velocity values assumed in our models lead to reasonably small kinetic power.

Finally, following the relation (17) from Bonito et al. (2007), we derive a jet mass loss rate ranging between $\dot{M} \sim 10^{-11} - 10^{-9}\ M_{\odot}$/yr. Once again, as discussed in details in Bonito et al. (2007), these results concerning both the kinetic power and the mass loss rate are several orders of magnitude lower than those observed in CO outflows and it seems reasonable that the simulated protostellar jets cannot drive molecular outflow.

4.2. Ejection rate of the blobs

Our simulations show that observable knots are mainly produced by the mutual interactions among blobs of plasma. We

---

[4] Corresponding to a physical radius of ≈ 70 AU.

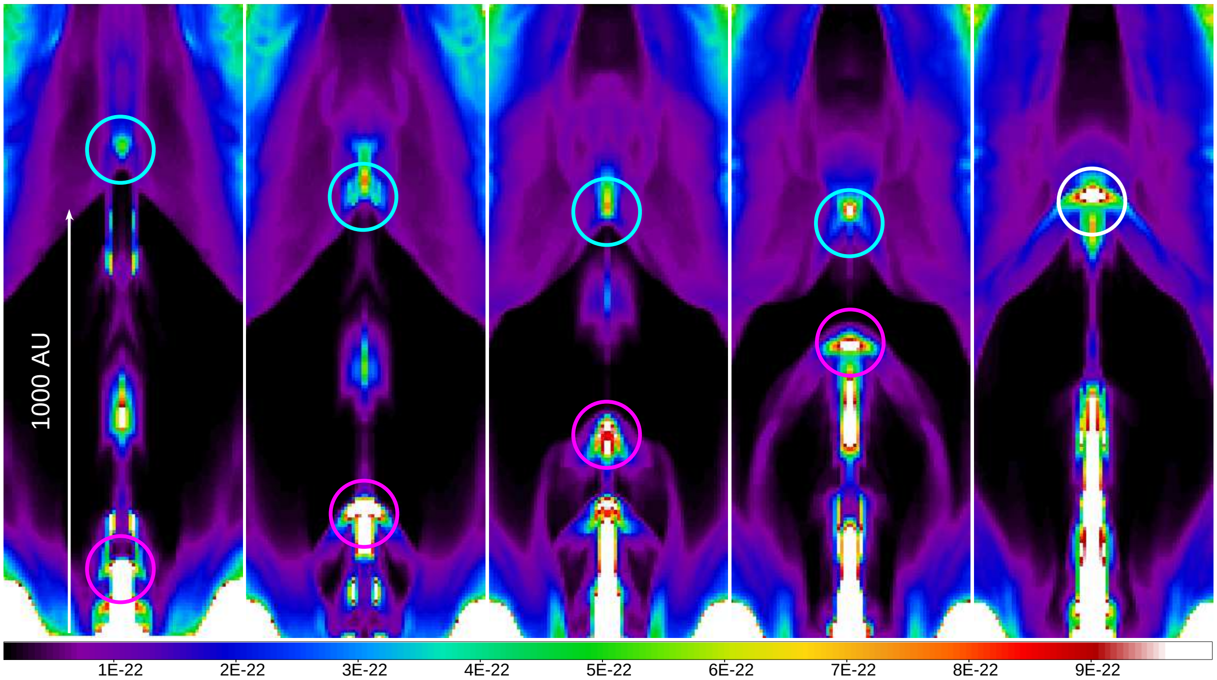

Figure 7. Evolution in a few years of the 2D spatial distributions of the density of the jet/ambient interaction in model LJ0.5: reverse shocks (highlighted by the cyan circle in each panel) form and travel in the direction opposite to the ejected blobs (highlighted by the magenta circle in each panel) and interact with them (white circle superimposed on the last panel).

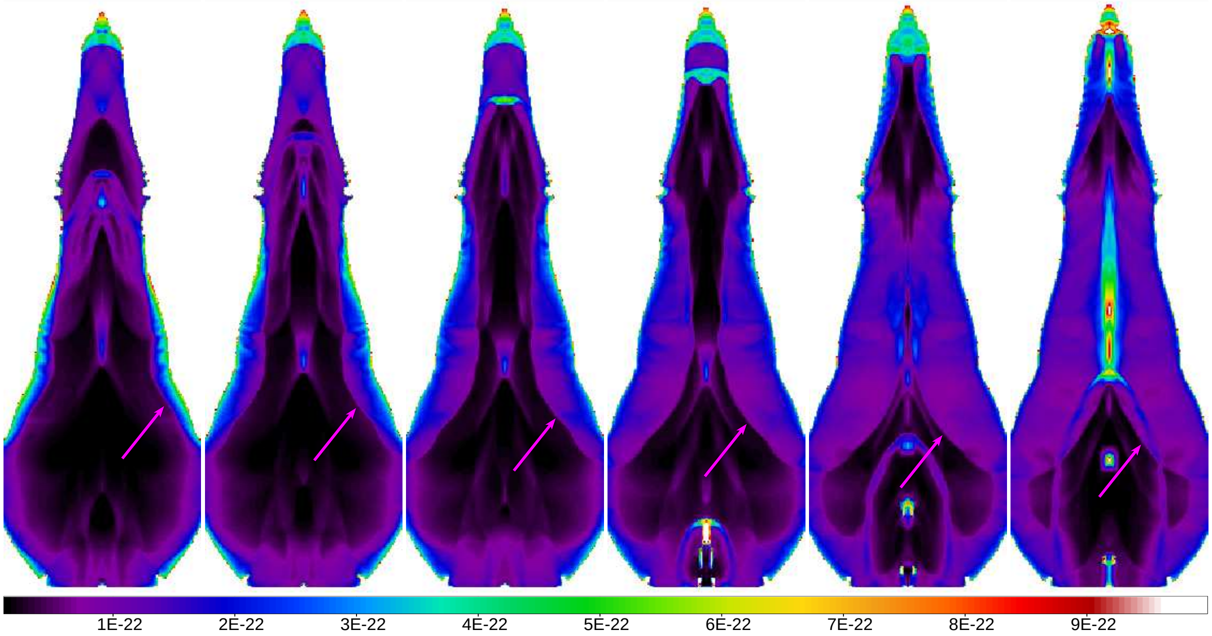

Figure 8. Model LJ8: evolution of the 2D spatial distributions of the density of the jet/ambient interaction (the first frame is after 70 yr and the last after 75 yr since the beginning of the jet/ambient interaction). Oblique shocks form (marked by the arrows in each panel) as the ejected blob interacts with the lateral cocoon.

expect, therefore, that the frequency of interactions between knots depends on the ejection rate of the blobs (see Sect. 2). In fact, from our exploration of the parameter Δt, we find that the knot interactions occur quite frequently in runs with high ejection rate (LJ05, and LJ2), whereas it is almost absent in the low ejection rate case (LJ8) over the timescale analyzed here. This result can be understood from the following simple estimation.

Bonito et al. (2007) showed that the observable velocity of a knot is a fraction of the initial jet velocity. This result is confirmed by our simulations: as discussed in Sect. 4.1, Fig. 10 shows that the maximum average speed of the knots along the

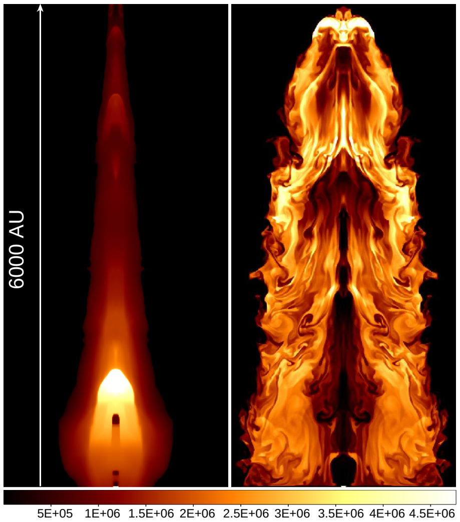

Figure 9. 2D spatial distributions of the temperature of the jet/ambient interaction in the $\Delta t = 2$ yr case: with radiative losses and thermal conduction after about 90 yr (left panel) and the pure radiative case after about 350 yr (right panel) of evolution. Ignoring the effects due to the thermal conduction, the whole computational domain is fully perturbed along the jet axis after more than 350 yr.

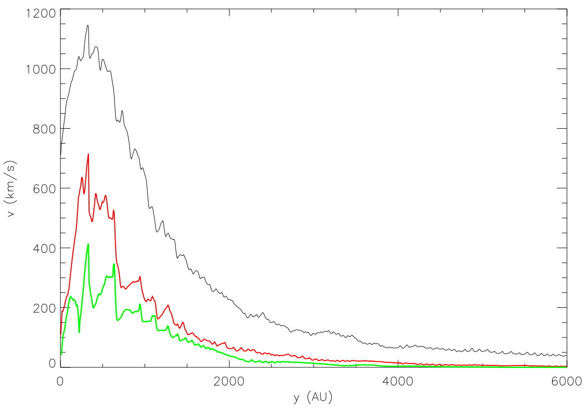

Figure 10. Average speed along the jet axis for the three runs LJ0.5, LJ2, and LJ8: the $\Delta t = 0.5$ yr case is in black, the $\Delta t = 2$ yr case is in red, and the $\Delta t = 8$ yr case is in green. The values of the knots speed derived from the runs are consistent with optical observations.

jet axis is a fraction of the initial average blob velocity (≈ 2000 km s^{-1}). The time at which we expect to observe a collision between two consecutive knots is

$$t_{\rm coll} = \frac{v_{\rm knot}}{\Delta v_{\rm knot}} (\Delta t)_{\rm knot} \tag{12}$$

where $\Delta v_{\rm knot}$ and $(\Delta t)_{\rm knot}$ are the average relative speed and the time interval between two consecutive knots, respectively. Both $v_{\rm knot}$ and $\Delta v_{\rm knot}$ are calculated assuming the same deceleration factor (since each knot velocity is a fraction of the initial blob speed); the latter is evaluated by considering only the blobs ejected with higher speed with respect to the previous ones. Since knots are produced mainly by the mutual interaction between blobs and between blobs and the ambient, we expect that $(\Delta t)_{\rm knot} \gtrsim \Delta t$. Considering Δt instead of $(\Delta t)_{\rm knot}$ in Eq. 12, we have, therefore, a lower limit on the collision time between knots. We derive that the interactions rises on average over about $t_{\rm coll} = 10, 30$, and more than 100 yr in runs LJ0.5, LJ2, and LJ8, respectively. This estimate explains the presence of knot interactions in the high ejection rate cases (LJ0.5 and LJ2) and the absence in the low ejection rate case (LJ8) over the timescale considered. In the light of the above discussion, we suggest, therefore, that the ejection rate might be constrained if the frequency of mutual interactions among ejected blobs can be determined from observations. The constrain of the ejection rate could be also interesting in the context of the accretion scenario. In fact it is believed that the ejection/accretion phenomena are intimately related, but a full description of this relation is still lacking.

5. Conclusions

We investigated the physical mechanism determining the irregular knotty structure of protostellar jets commonly observed in the optical band, and recently also detected in X-rays (e.g. HH 154, Favata et al. 2006). To this end, we developed a numerical model describing a pulsed jet, consisting of a chain of blobs, each ejected along the jet axis with random initial velocity, and traveling in an initial homogeneous ambient medium. Our simulations represent the first attempt to model a pulsed jet that simultaneously includes the thermal conduction and the radiative losses processes. In particular, we find that the thermal conduction plays a crucial role in damping out the hydrodynamic instabilities that would develop within the cocoon. Since these instabilities contribute to break the jet, the thermal conduction makes the jet to propagate to larger distances.

The jet is modeled both as an initial light jet (a scenario which seems likely to describe the observations of HH 154, both in X-rays and in the optical band; Bonito et al. 2008) and as an initial heavy jet. In all the cases, we find that the interactions among subsequent ejected blobs are a common feature to our simulations. As a result of these interactions, each new ejected blob travels through a strongly inhomogeneous medium characterized by density and thermal conditions largely varying along the jet axis; as a result, the density contrast between the blob and the surrounding medium varies during the jet/ambient evolution and the different pre-shock conditions leads to strong variations of the shock velocities and of the post-shock properties.

The mutual interactions among the blobs lead to a variety of density structures within the jet not described by current models of jets (however see Yirak et al. 2009). These structures determine a rather complex morphology of the jet. The most relevant are: single high speed knots, showing a measurable proper motion in nice agreement with optical and X-rays observations; irregular chains of knots aligned along the jet axis, and possibly interacting with each other, consistent with observations of several protostellar jets; reverse shocks interacting with outgoing knots; oblique shock patterns produced by the reflection of shocks at the cocoon surrounding the jet. We also found that the range of velocity of the knots formed from mutual interactions among blobs is consistent with the typical range of values observed (e.g. Reipurth & Bally 2001).

We explored the effects of the ejection rate of the blobs on the evolution of the density and temperature spatial distributions of the jet/ambient interaction. The frequency of interactions between formed knots depends on the ejection rate. We suggest, therefore, that the comparison between our model results and the observations may give some hints on the ejection rate of protostellar jets. Since the opposite and complementary processes of accretion of mass onto a star and ejection of mass from a star are commonly assumed to be related, from the constraints on the ejection rate we may also infer important physical information on the accretion rates.

We expect some details of our model to depend on the assumption of the exponential distribution for the ejection velocity of each blob (determined with a given random seed). From a quantitatively point of view, the single blob velocity can change with a different random seed and also the energetic and dynamics of particular structures is expected to vary if different velocity distributions are chosen. Nevertheless, in any case we expect to obtain the main features discussed here, namely the formation of shock fronts, the collision among knots due to blobs ejected at different epochs with different speed, the interaction among knots and reverse shocks.

The model of a randomly ejected pulsed jet is, therefore, a promising scenario to explain the physical mechanism leading to the irregular knotty structure observed within protostellar jets in a wide range of wavelengths, from optical to X-rays. Further development of this work will be reported in a forthcoming paper (Bonito et al., 2009, in preparation) where we will investigate the morphology and variability of X-ray emitting structures formed within the randomly ejected pulsed jet.

Acknowledgements. We would like to thank the referee, Dr. A. C. Raga, for his helpful comments and suggestions. R.B., S.O., M.M, and G.P. acknowledge support by the Marie Curie Fellowship Contract No. MTKD-CT-2005-029768. The software used in this work was in part developed by the DOE-supported ASC/Alliances Center for Astrophysical Thermonuclear Flashes at the University of Chicago, using modules for thermal conduction and optically thin radiation constructed at the Osservatorio Astronomico di Palermo. The calculations were performed at CINECA (Bologna, Italy) and on the cluster at the SCAN (Sistema di Calcolo per l'Astrofisica Numerica) facility of the INAF – Osservatorio Astronomico di Palermo.

References

Bally, J., Feigelson, E., & Reipurth, B. 2003, ApJ, 584, 843
Bodo, G., Massaglia, S., Ferrari, A., & Trussoni, E. 1994, A&A, 283, 655
Bonito, R., Fridlund, C. V. M., Favata, F., et al. 2008, A&A, 484, 389
Bonito, R., Orlando, S., Peres, G., Favata, F., & Rosner, R. 2004, A&A, 424, L1
Bonito, R., Orlando, S., Peres, G., Favata, F., & Rosner, R. 2007, A&A, 462, 645
Borkowski, K. J., Shull, J. M., & McKee, C. F. 1989, ApJ, 336, 979
Colella, P. & Woodward, P. R. 1984, Journal of Computational Physics, 54, 174
Cowie, L. L. & McKee, C. F. 1977, ApJ, 211, 135
Dalton, W. W. & Balbus, S. A. 1993, ApJ, 404, 625
Eislöffel, J. & Mundt, R. 1998, AJ, 115, 1554
Eislöffel, J., Mundt, R., & Böhm, K. 1994, AJ, 108, 1042
Favata, F., Bonito, R., Micela, G., et al. 2006, A&A, 450, L17
Favata, F., Fridlund, C. V. M., Micela, G., Sciortino, S., & Kaas, A. A. 2002, A&A, 386, 204
Fridlund, C. V. M. & Liseau, R. 1998, ApJ, 499, L75
Fridlund, C. V. M., Liseau, R., Djupvik, A. A., et al. 2005, A&A, 436, 983
Fryxell, B., Olson, K., Ricker, P., et al. 2000, ApJS, 131, 273
Garatti, A. C. o., Eislöffel, J., Froebrich, D., et al. 2009, ArXiv e-prints
Giuliani, J. L. 1984, ApJ, 277, 605
Hartigan, P., Morse, J. A., Reipurth, B., Heathcote, S., & Bally, J. 2001, ApJ, 559, L157
Hartigan, P. M. 2003, in Revista Mexicana de Astronomia y Astrofisica, vol. 27, Vol. 15, Revista Mexicana de Astronomia y Astrofisica Conference Series, ed. J. Arthur & W. J. Henney, 112–114
Kaastra, J. S. & Mewe, R. 2000, in Atomic Data Needs for X-ray Astronomy, p. 161
MacNeice, P., Olson, K. M., Mobarry, C., de Fainchtein, R., & Packer, C. 2000, Computer Physics Communications, 126, 330
Mewe, R., Gronenschild, E. H. B. M., & van den Oord, G. H. J. 1985, A&AS, 62, 197
Orlando, S., Peres, G., Reale, F., et al. 2005, A&A, 444, 505
Podio, L., Bacciotti, F., Nisini, B., et al. 2006, A&A, 456, 189
Raga, A. C. 1992, MNRAS, 258, 301
Raga, A. C., de Colle, F., Kajdič, P., Esquivel, A., & Cantó, J. 2007, A&A, 465, 879
Raymond, J. C. & Smith, B. W. 1977, ApJS, 35, 419
Reipurth, B. & Bally, J. 2001, ARA&A, 39, 403
Reipurth, B., Heathcote, S., Yu, K. C., Bally, J., & Rodríguez, L. F. 2000, ApJ, 534, 317
Roberts, D. A. 1986, ApJ, 300, 568
Spitzer, L. 1962, Physics of Fully Ionized Gases (New York: Interscience, 1962)
Vitorino, B. F., Jatenco-Pereira, V., & Opher, R. 2002, A&A, 384, 329
Yirak, K., Frank, A., Cunningham, A. J., & Mitran, S. 2009, ApJ, 695, 999